GEODINAMICA ACTA
2018, VOL. 30, NO. 1, 1–14
https://doi.org/10.1080/09853111.2017.1408264

Taylor & Francis
Taylor & Francis Group

OPEN ACCESS Check for updates

Slip distribution and source parameters of the 20 July 2017 Bodrum-Kos earthquake (Mw6.6) from GPS observations

İ Tiryakioğlu[a,b], B. Aktuğ[c], C. Ö. Yiğit[d], H. H. Yavaşoğlu[e], H. Sözbilir[f,g], Ç Özkaymak[b,h], F. Poyraz[i], E. Taneli[a], F. Bulut[j], A. Doğru[j] and H. Özener[j]

[a]Faculty of Engineering, Department of Geomatics Engineering, Afyon Kocatepe University, Afyon, Turkey; [b]Earthquake Research and Implementation Center, Afyon Kocatepe University, Afyon, Turkey; [c]Faculty of Engineering, Department of Geophysical Engineering, Ankara University, Ankara, Turkey; [d]Faculty of Engineering, Department of Geomatics Engineering, Gebze Technical University, Gebze-Kocaeli, Turkey; [e]Faculty of Civil Engineering, Department of Geomatics Engineering, Istanbul Technical University, Istanbul, Turkey; [f]Department of Geology, Dokuz Eylul University, Izmir, Turkey; [g]Earthquake Research and Implementation Center, Dokuz Eylul University, Izmir, Turkey; [h]Faculty of Engineering, Department of Geology Engineering, Afyon Kocatepe University, Afyonkarahisar, Turkey; [i]Faculty of Engineering, Department of Geomatics Engineering, Cumhuriyet University, Sivas, Turkey; [j]Department of Geodesy, Kandilli Observatory and Earthquake Research Institute, Bogazici University, Istanbul, Turkey

ABSTRACT

Greek-Turkish boundary near the cities Kos and Bodrum has been shaken on July 20, 2017 by a Mw6.6 earthquake. The mainshock is located offshore and did not generate an on-land surface rupture. Analyzing pre- and post-earthquake continuous/survey-type static GPS observations, we investigated co-seismic surface displacements at 20 sites to characterize source parameters and slip-distribution of the mainshock. Fault plane solutions as well as co-seismic slip distribution have been acquired through the inversion of co-seismic GPS displacements modeling the event as elastic dislocations in a half space. Fault plane solution shows a southward dipping normal-type fault segment extending a depth down to ~12 km, which remains within the brittle upper crust. Results from the distributed slip inversion show that the mainshock activated a ~65 km fault section, which has three high slip patches, namely western, central and eastern patches, where the coseismic slips reach up to 13, 26, and 5 cm, respectively. This slip pattern indicates that the pre-earthquake coupling, which is storing the slip deficit, occurred on these three patches.

ARTICLE HISTORY
Received 18 August 2017
Accepted 20 November 2017

KEYWORDS
GPS; co-seismic; The 20 July 2017 Bodrum-Kos earthquake (Mw6.6); slip; rupture process

1. Introduction

The southwestern Anatolia is characterized by a tectonically active N-S directed extensional tectonic regime, where several E-W and WNW-ESE trending Plio-Quaternary grabens have developed, such as Gökova Graben (the Gulf of Gökova), Büyük Menderes Graben and Gediz Graben (Dewey & Şengor, 1979; Jackson & McKenzie, 1984; McKenzie, 1972; Sengor, 1987). Its extensional character has been verified by many studies investigating the mechanism of fault systems in this region by using GPS data (Aktug, Kaypak, & Çelik, 2010; Aktug et al., 2009; Dogru, Gorgun, Ozener, & Aktug, 2014; McClusky et al., 2000; Ozener, Dogru, & Acar, 2013; Reilinger et al., 2006; Tiryakioglu et al., 2013).

20 July 2017 Bodrum-Kos earthquake (Mw6.6 – 01:31 UTC) occurred along the western section of the Gökova Gulf, between the cities of Bodrum and Kos. The rupture zone cannot be seen directly since the earthquake is located offshore and did not generate any on-land rupture. Therefore, resolving the nodal plane from auxiliary plane is an ambiguity in seismological solutions. In this case, GPS-derived coseismic displacements are of great importance for modeling the source parameters and the slip distribution of the mainshock. In this study, co-seismic surface displacements are converged to characterize source parameters and the slip distribution of the 2017 Bodrum-Kos Earthquake (Mw 6.6) assuming a finite dislocation plane in an elastic half-space.

We used 15 continuous GPS and 5 campaign-surveyed GPS stations to capture coseismic displacement during the 2017 Bodrum-Kos Earthquake (Mw6.6). The cGPS data covers three days before and three days after the mainshock. Obtained coseismic surface displacements at 20 sites are analyzed to characterize source parameters and slip distribution of the 2017 Bodrum-Kos Earthquake (Mw6.6).

CONTACT H. Özener ozener@boun.edu.tr

© 2017 The Author(s). Published by Informa UK Limited, trading as Taylor & Francis Group.
This is an Open Access article distributed under the terms of the Creative Commons Attribution License (http://creativecommons.org/licenses/by/4.0/), which permits unrestricted use, distribution, and reproduction in any medium, provided the original work is properly cited.

2. Seismotectonic setting

The Aegean region, is seismically one of the most active and rapidly extending regions on the Earth, has been deformed under the control of an N–S extensional tectonic regime at a rate reaching up to 30/40 mm/yr since the Pliocene (Bozkurt, 2001; Brun et al., 2016; Dewey & Şengor, 1979; Jackson & Mckenzie, 1984; Jolivet & Brun, 2010; Kaymakci, 2006; Kocyigit & Deveci, 2007; Le Pichon, Chamot-Rooke, Lallemant, Noomen, & Veis, 1995; Sozbilir, Sari, Uzel, Sumer, & Akkiraz, 2011; Yilmaz et al., 2000). There are two basic mechanisms explaining the extension of the Aegean region. The first explanation is built on the southwestern escape of the Anatolian plate (McKenzie, 1972) in response to convergent movement of the Arabia–Africa and Eurasian plates along the Bitlis collision zone (Dewey & Şengor, 1979). An alternative explanation is based on the framework of the northward-moving Arabian plate and the rollback of the Hellenic subduction zone where the African lithosphere is subducted below the Aegean Sea (McClusky et al., 2000). This extensional field resulted in approximately E-W trending depressions in SW Anatolia (Bozkurt, 2001; Ciftci & Bozkurt, 2010; Kaymakci, 2006; Ozkaymak, Sozbilir, & Uzel, 2013).

The Gulf of Gökova is one of E-W trending asymmetric depression with 120 km long and widens westward from 5 to 30 km. It is developed on the Lycian nappes, filled with Plio-Quaternary terrestrial and marine sediments (Gurer, Sangu, Ozburan, Gurbuz, & Sarica-Filoreau, 2013) and is bordered by Datça Peninsula to the south, the island of Kos to the west, and Bodrum Peninsula to the North. The northern margin of the Gulf is controlled by the Gökova Fault Zone (GFZ), is seismically one of the most active structures in SW Anatolia. It is a E-W to NE-SW trending broad arc-shaped zone that formed the northern breakaway fault of the Gökova Gulf (Figure 1). Along much of its onshore lengths, GFZ has well-developed surface geomorphological expressions and geological features such as fresh fault surface that observed on triangular facets. Field-based studies suggest that GFZ is defined by south-dipping, high angle (70°–85°) normal faults (Gurer et al., 2013). Several marine-based

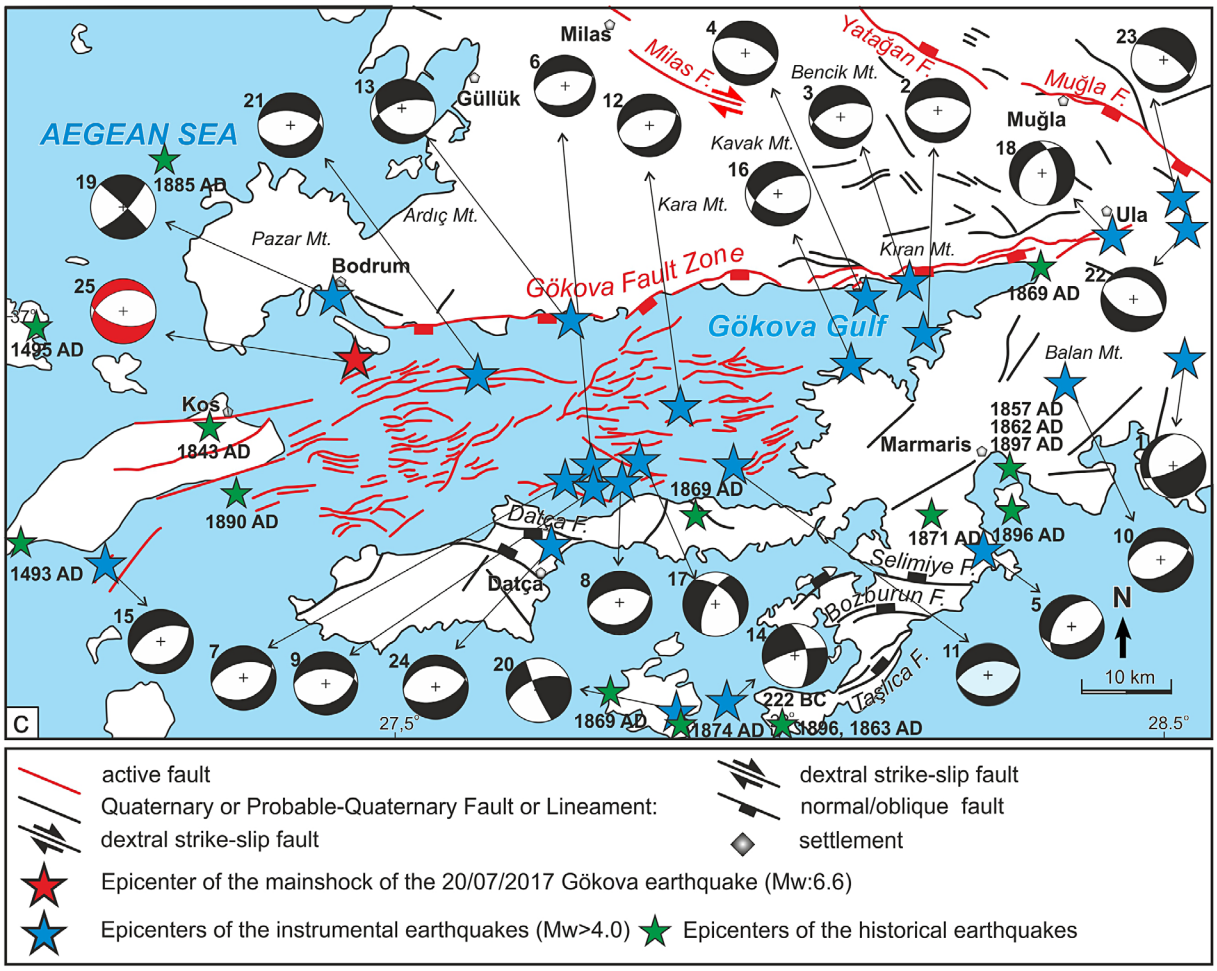


Figure 1. Seismotectonic map of the Gökova Gulf region, showing the epicenters of both instrumental period and historical earthquakes. For the details and numbering of instrumental earthquakes, see Table 1. The focal mechanism solution and the epicenter of the earthquakes are taken from McKenzie (1972); Yolsal, Taymaz, and Helvaci (2014); This study; National Observatory of Athens, Geodynamic Institute (NOA, 2017); GeoForschungsZentrum (GFZ-Potsdam, 2017); Kandilli Observatory and Earthquake Research Institute (KOERI, 2017); European Mediterranean Seismological Centre (EMSC, 2017); The Harvard Centroid Moment Tensor Catalog (HRV, 2017); Disaster and Emergency Management Presidency (DDA, 2017).

geophysical surveys have been carried out in the Gulf of Gökova in order to delineate fault systems of this region (Iscan, Tur, & Gokasan, 2013; Kurt, Demirbag, & Kuscu, 1999; Tur, Yaltirak, Elitez, & Sarikavak, 2015; Ulug, Duman, Ersoy, Ozel, & Avci, 2005). According to the results obtained from these surveys (Figure 1), the GFZ runs E-W parallel to the coast in the eastern part of Gökova Gulf from Akyaka to Ören, where it makes a left bend and continues west-southwestward that splay into several submarine fault strands displaying an anastomosing pattern, where there is a number of second order faults between the seismic segments (Figure 2). Thus, in the Gulf of Gökova, the GFZ begins to lose its single fault line character and splays into a complex fault pattern. The complexity of the GFZ in the Gulf may actually be related to the interaction between deep-seated strike-slip faults and shallow-seated normal faults which characterize the SW Anatolia neotectonic regime. According to geological markers observed in this study, the total offset of GFZ is about 1000 m since the Plio-Quaternary. This suggests a slip rate of 0.2 mm/yr.

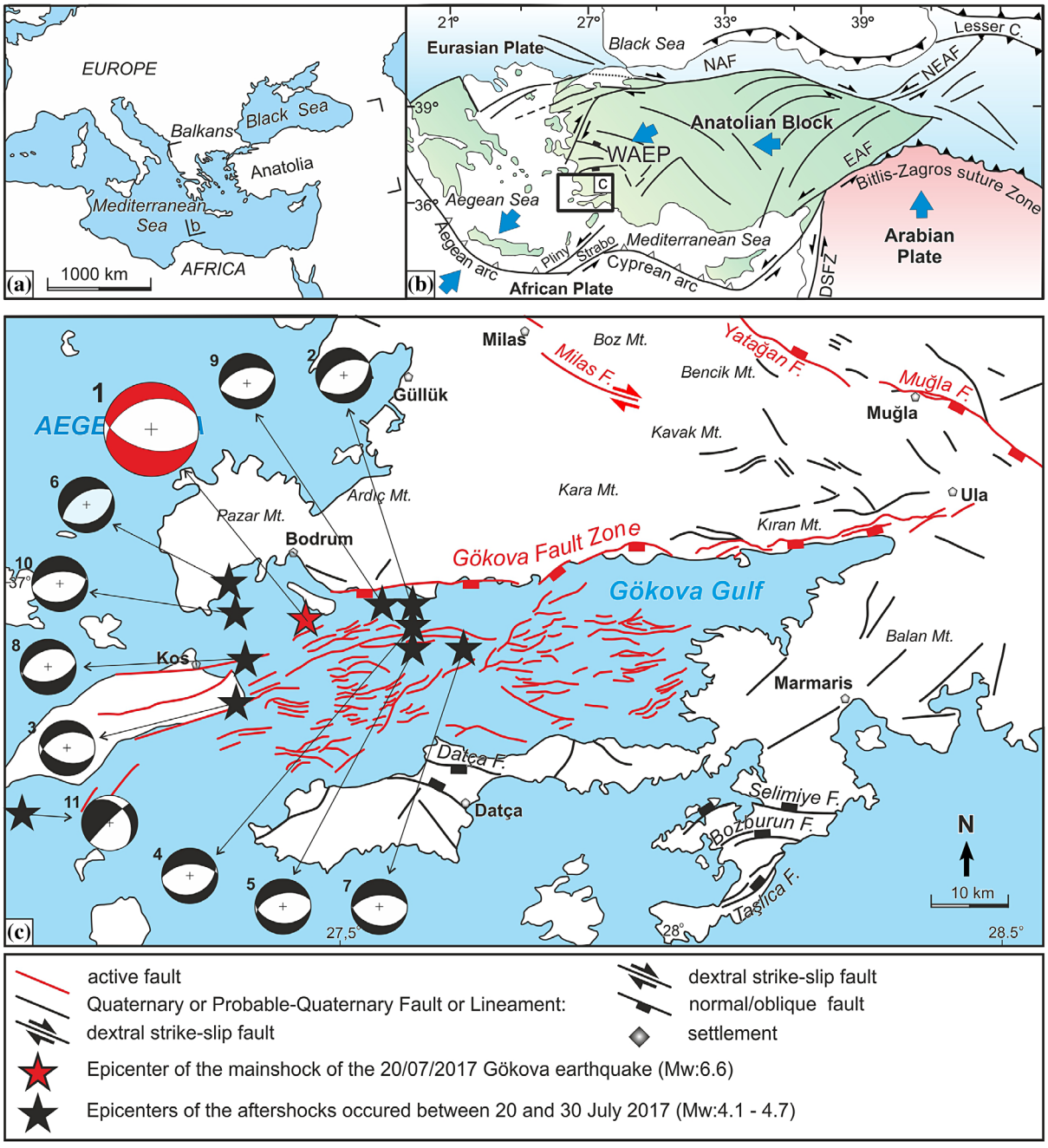


Figure 2. (a) Location of the Anatolia at a global scale, (b) Tectonic outline of the eastern Mediterranean area (compiled from Kaymakci, 2006 and Ozkaymak, 2015;). Abbreviations: WAEP, West Anatolian Extensional Provinces; DSFZ, Dead Sea Fault Zone; EAF, East Anatolian Fault; NAF, North Anatolian Fault; NEAF, Northeast Anatolian Fault. (c) Simplified active fault map of Northwest Anatolia and available focal mechanism solutions of mainshock and the aftershocks of the 20 July 2017 Bodrum-Kos earthquake (Mw6.6) (Focal mechanism solution (FMS) of earthquakes are taken from EMSC earthquake catalog. For the numbering of the earthquakes, see Table 2. Fault data are taken from Konak & Senel, 2002; Duman, Emre, Ozalp, & Elmacı, 2011; Emre, Duman, & Ozalp, 2011; Iscan et al., 2013).

In recent and historical times, a number of moderate to major destructive earthquakes have struck the Gökova region due to activity on seismic segments of GFZ (Figure 1, Table 1). Historical seismicity in the region are widely reported by specifying damages of destructive earthquakes such as 24 BC, 412 BC (Ambraseys & White, 1997), 227 BC, 199–198 BC, AD 142–144, 174, AD 344, AD 474–478 and AD 554–558, 1493 1851, 1863, and 1869 events (Guidoboni, Comastri, & Triana, 1994; Yolsal, Taymaz, & Yalciner, 2007). In 1493, the town of Bodrum was totally destroyed (Luttrell, 1999). The major earthquake-induced Eastern Mediterranean tsunamis were developed in 365, 554, 1303, 1481, 1494, 1822 and 1948 earthquake (Altinok & Ersoy, 2000; Yolsal & Taymaz, 2012; Yolsal et al., 2007). Stiros (2000) also emphasized the correlation between the eruptive volcanic and intense earthquake activities on Nisyros island in AD 1887, 1873 and possibly around 1422. According to the Yolsal et al. (2007), there are so strong tsunami events, where the wave heights are recorded on coastal plains up to 3 m, in the eastern Mediterranean with a recurrence interval of about 150–250 years.

Recent studies based on surface morphology, fault mechanism solutions, seismicity and marine seismic reflection data (Eyidogan, Akinci, Gündogdu, Polat, & Kaypak, 1996; Gorur et al., 1995; Kurt et al., 1999; Saroglu, Emre, & Kuşçu, 1992; Ulug et al., 2005; Yolsal & Taymaz, 2010) provide evidence for instrumental activity of GFZ (Figure 1). These include the earthquakes of 23 April 1933 (Mw6.2), 23 May 1941 (Mw5.4), 13 December 1941 (Mw6.3), 25 April 1959 (Mw6.1), 19 February 1989 (Mw5.6), 5 October 1999 (Mw5.2), 4 August 2004 (Mw5.4), and 10 January 2005 (Mw5.2) earthquakes. The released energy is predominantly in swarm type in Gökova region as observed during 2004 and 2005 earthquakes (Kalafat & Horasan, 2012). The last destructive earthquake struck at 1:31 am local time near the Kos (Greece), and Bodrum (Turkey) with the magnitude of 6.6 (KOERI, 2017).

2.1. The 20th July 2017 Bodrum-Kos earthquake

20 July 2017 Bodrum-Kos earthquake (Mw6.6) occurred at 01:31 (UTC) and ruptured a fault section along the western Gökova Gulf, between the cities of Bodrum and Kos (Figure 2, Table 2). The mainshock resulted in two fatalities in the Kos island. It caused also some damage due to the tsunami along the southern coast of Bodrum Peninsula as well as the northern coast of Kos island. 13 cm wave-height was measured at Bodrum sea-level station. After the earthquake, 30–40 cm wave-height was observed on the Bodrum shores. The tsunami caused floods in some areas and reached heights of up to 1.9 m.

(KOERI-RETMC preliminary report – the 2017 Bodrum-Kos earthquake, found at http://www.koeri.boun.edu.tr/sismo).

After that mainshock, about a dozen of aftershocks were recorded throughout the Gökova Gulf (Figure 2, Table 3). The global focal mechanism solutions suggest that an approximately E-W trending fault generated the earthquake with a pre-dominant normal-type slip. The northern border of the Gökova Gulf, where the epicenters of earthquakes are aligned, is seismotectonically controlled by GFZ.

Table 1. List of the instrumental period earthquakes occurred along the Gökova Fault Zone. References (1): McKenzie (1972); (2): Yolsal et al. (2014); (3): HRV (2017); (4): EMSC (2017); (5): DDA (2017); (6): NOA (2017); (7): GFZ-Potsdam (2017); (8): KOERI (2017); (9): This study. Abbreviations D: Depth; R: References.

No	Date	Time (UTC)	Longitude	Latitude	Magnitude (Mw)	*D* (km)	*R*
1	23.04.1933	05:57:37	27.29	36.77	6.2	30	1,2
2	23.05.1941	23:00:48	28.35	37.22	5.4	48	1,2
3	13.12.1941	06:16:05	28.06	37.13	6.3	30	1,2
4	25.04.1959	00:26:39	28.50	36.97	5.9	50	1,2
5	19.02.1989	14:28:45	28.19	36.98	5.4	15	1,2
6	27.04.1989	23:06:52	28.16	37.03	5.1	14	2,3
7	28.04.1989	13:30:19	28.10	37.02	5.4	8	2,3
8	05.10.1999	00:53:27	28.23	36.75	5.2	14	2,3
9	03.08.2004	13:11:30	27.77	36.85	5.1	11	2,3
10	04.08.2004	03:01:05	27.76	36.83	5.4	9	2,3
11	04.08.2004	04:19:46	27.81	36.83	5.3	13	2,3
12	04.08.2004	14:18:48	27.78	36.84	5.2	8	2,3
13	20.12.2004	23:02:14	28.36	36.93	5.3	8	2,3
14	10.01.2005	23:48:49	27.92	36.85	5.2	8	2,3
15	11.01.2005	04:35:56	27.87	36.89	5.2	10	2,3
16	07.09.2010	14:18:00	27.73	37.02	4.0	2	4,5
17	08.08.2010	00:24:12	27.92	36.61	4.1	14	4,6
18	08.05.2011	06:50:24	27.24	36.70	5.1	11	4,7
19	04.06.2012	14:19:53	28.16	36.94	4.5	6	4,6
20	26.11.2012	17:35:42	27.95	36.58	4.7	22	4,8
21	16.05.2013	03:02:01	28.39	37.05	4.8	8	4,8
22	15.08.2014	04:00:17	27.43	37.01	4.0	10	4,8
23	21.06.2013	18:26:41	27.87	36.54	4.2	86	4,8
24	29.05.2015	08:02:51	27.61	36.92	4.0	7	4,8
25	15.12.2016	16:43:56	28.64	37.09	4.0	7	4,5
26	13.04.2017	16:22:15	28.66	37.14	4.9	5	4,8
27	25.01.2017	01:19:32	27.66	36.79	4.0	10	4,5
28	20.07.2017	22:31:11	27.45	36.96	6.6	6	9

Table 2. Focal mechanism solutions for the mainshock of the 20/07/2017 Bodrum-Kos earthquake (Mw6.6) from various seismology centers and GPS (this study).

			Nodal Plane 1			*Nodal Plane 2*					
Model	Lon. (°)	Lat. (°)	Strike (°)	Dip (°)	Rake (°)	Strike (°)	Dip (°)	Rake (°)	Depth (km)	M_0 (dyn*m)	M_w
This Study (GPS)[a]	27.368	36.946	105	57	−62	–	–	–	8.8	$1.09\ 10^{26}$	6.6
USGS	27.414	36.925	84	53	−103	285	39	−73	11.5	$1.13\ 10^{26}$	6.6
KOERI	27.405	36.962	78	40	−112	286	53	−72	6	$1.13\ 10^{26}$	6.6
NOA	27.433	36.964	102	48	−79	265	43	−102	6	$1.13\ 10^{26}$	6.6
GFZ-Potsdam	27.510	36.960	270	56	−94	98	35	−82	11	$9.70\ 10^{25}$	6.6
AFAD	27.443	36.920	286	38	−80	82	53	−98	19.4	–	6.5

[a]The depth is given as the midpoint of the computed rectangular fault. The coordinates are the western endpoint of the fault.

Table 3. List of the mainshock and aftershocks of the 20/07/2017 Bodrum-Kos earthquake (Mw6.6) Epicentral locations are taken from EMSC earthquake catalog except for the mainshock. References (1): This study; (2): NOA; (3): GFZ-Potsdam; (4): KOERI. Abbreviations D: Depth; R: References.

No.	Date	Time (UTC)	Longitude	Latitude	Magnitude (Mw)	*D* (km)	*R*
1	20.07.2017	22:31:11	27.45 E	36.96 N	6.6	6	1
2	21.07.2017	01:35:44	27.60 E	36.93 N	4.3	7	2
3	21.07.2017	02:12:34	27.37 E	36.86 N	4.7	9	3
4	21.07.2017	03:59:01	27.61 E	36.92 N	4.4	6	3
5	21.07.2017	05:14:00	27.61 E	36.91 N	4.3	5	3
6	21.07.2017	05:52:13	27.34 E	36.98 N	4.1	4	3
7	21.07.2017	09:55:54	27.68 E	36.91 N	4.4	10	3
8	21.07.2017	17:09:48	27.34 E	36.91 N	4.7	11	4
9	21.07.2017	21:05:04	27:57 E	36.93 N	4.6	6	3
10	22.07.2017	17:09:21	27.35 E	36.96 N	4.4	11	4
11	22.07.2017	17:25:47	26.75 E	36.58 N	4.7	140	4

3. Geodetic networks data and modeling

3.1. Geodetic networks in southwest Turkey and processing

Geodesy is conventionally a useful approach to understand the faulting processes using slip rate of the interseismic, pre-seismic, coseismic and postseismic deformations (Lisowski, 1997; Reddy & Sunil, 2008; Reilinger, McClusky, Paradissis, Ergintav, & Vernant, 2010; Reilinger et al., 2006; Tiryakioglu, 2015; Tiryakioglu, Yigit, Yavaşoglu, Saka, & Alkan, 2017). For this purpose, InSAR, GPS, SLR and VLBI techniques have been developed since the early 1980s. In this study, coseismic deformation has been investigated by analyzing GPS data.

The combined geodetic network consists of 15 continuous and 5 campaign-surveyed GPS stations (Figure 3(a)). Five continuous stations (YALI, ORTA, TGRT, TRKB and MUMC) have been installed at Bodrum town of Mugla. They are operated by Independent Geomatic Engineers Office-Bodrum. These stations are located at ~13.5, 15.5, 17, 23 and 30 km to the mainshock epicenter, respectively. Seven continuous stations (DATC, DIDI, MUG1, AYD1, FETH, CESM and IZMI) have been selected from the network of Continuously Operating Reference Stations, Turkey (CORS-TR). The distances of these stations to the mainshock epicenter are ~30, 51, 90, 108, 156, 165 and 183 km, respectively. Three continuous stations (RODO, ROD1 and KALY) have been installed at Rhodes in Greece. The distances of these stations to the mainshock epicenter are ~90, 110 and 40 km, respectively. In this area, 5 campaign-surveyed GPS stations (BODR, KNID, CAMK, MARM, KYCZ) have been measured during five GPS campaigns between 2002 and 2013. The distances of these stations to the mainshock epicenter are 10, 27, 48, 51 and 108 km, respectively (Tiryakioglu et al., 2013). The five campaign-surveyed GPS stations were re-surveyed on 24 July 2017 (three days following the mainshock). All stations were recorded at a 30-s sampling rate. Elevation cut-off angles were fixed at 10-degree. These networks have been originally established for surveying cadastral geometry, transportation, construction, emergency management and also monitoring of the tectonic motions.

After the 2017 Bodrum-Kos mainshock (20 July 2017, Mw6.6, KOERI, 2017), the data dated from 19 to 23 July 2017 by 20 stations of the networks near the Bodrum-Kos earthquake epicenter was obtained immediately. More than 3000 aftershocks were recorded by the KOERI in the first 3 days ranging between magnitudes of 2.0 and 5.0 (Figure 3).

2-day data including pre-seismic and coseismic deformation from 20 stations were recorded at 30s intervals in RINEX format. The precise coordinates of the stations were estimated using GAMIT/GLOBK software. To process the data with GAMIT software, the rapid orbit information, earth rotations parameters and antenna information were obtained from Scripps Orbit and Permanent Array Centre (SOPAC). Moreover, the antenna phase center was derived according to the height-dependent model. During the analysis, LC (L3), which is the ionosphere-independent linear combination of the L1 and L2 carrier waves and the

Table 4. Observed surface displacements and standard errors at GPS sites.

Site	Λ (°)	ϕ (°)	Δe (mm)	Δn (mm)	$\sigma_{\Delta e}$ (mm)	$\sigma_{\Delta n}$ (mm)	Δh (mm)	σ_h (mm)
YALI	36.9950	27.5353	7.2	***153.0***	2.7	2.8	7.5	10.9
ORTA	37.0508	27.3487	***−39.4***	***100.3***	2.4	2.6	14.7	9.5
MUMC	37.1387	27.6190	***23.3***	***69.1***	2.5	2.8	4.2	9.9
TRKB	37.1139	27.3226	***−24.9***	***64.9***	2.3	2.4	3.1	9.1
TGRT	37.0071	27.2568	***−9.2***	***24.8***	2.9	3.1	0.8	11.5
MARM	36.7726	27.9628	6.1	−2.0	2.7	2.8	6.0	10.1
KYCZ	36.9788	28.6864	12.0	5.8	9.1	9.4	9.8	30.3
KNID	36.6822	27.3939	***−20.0***	***−49.0***	3.9	4.4	−2.3	16.3
CAMK	37.1965	27.8358	2.0	***28.0***	4.6	5.7	28.0	20.7
BODR	37.0190	27.4010	***−38.3***	***160.2***	9.1	9.2	119.1	22.5
DATC	36.7086	27.6918	***12.2***	***−33.7***	3.5	3.8	6.4	13.9
DIDI	37.3721	27.2687	−5.9	***18.9***	2.6	2.7	−4.0	9.8
MUG1	37.2143	28.3557	3.9	−9.6	3.8	3.9	1.2	14.2
FETH	36.6262	29.1238	−1.5	1.8	3.3	3.4	−5.3	12.7
AYD1	37.8407	27.8379	1.8	4.4	3.9	4.1	−7.5	15.5
CESM	38.3038	26.3726	0.0	1.1	2.9	3.1	−6.2	11.0
IZMI	38.3948	27.0818	0.7	0.9	2.7	2.8	−1.6	10.4
RODO	36.4023	28.1953	−0.5	−0.6	2.5	2.6	−0.3	9.8
ROD2	36.0209	27.9232	2.3	−5.5	2.5	2.5	6.4	9.6
KALY	36.9624	26.9617	3.9	−2.5	2.8	3.0	5.2	11.5

*Bold and italicized value represents statistically significant coseismic displacement with respect to 3-sigma threshold.

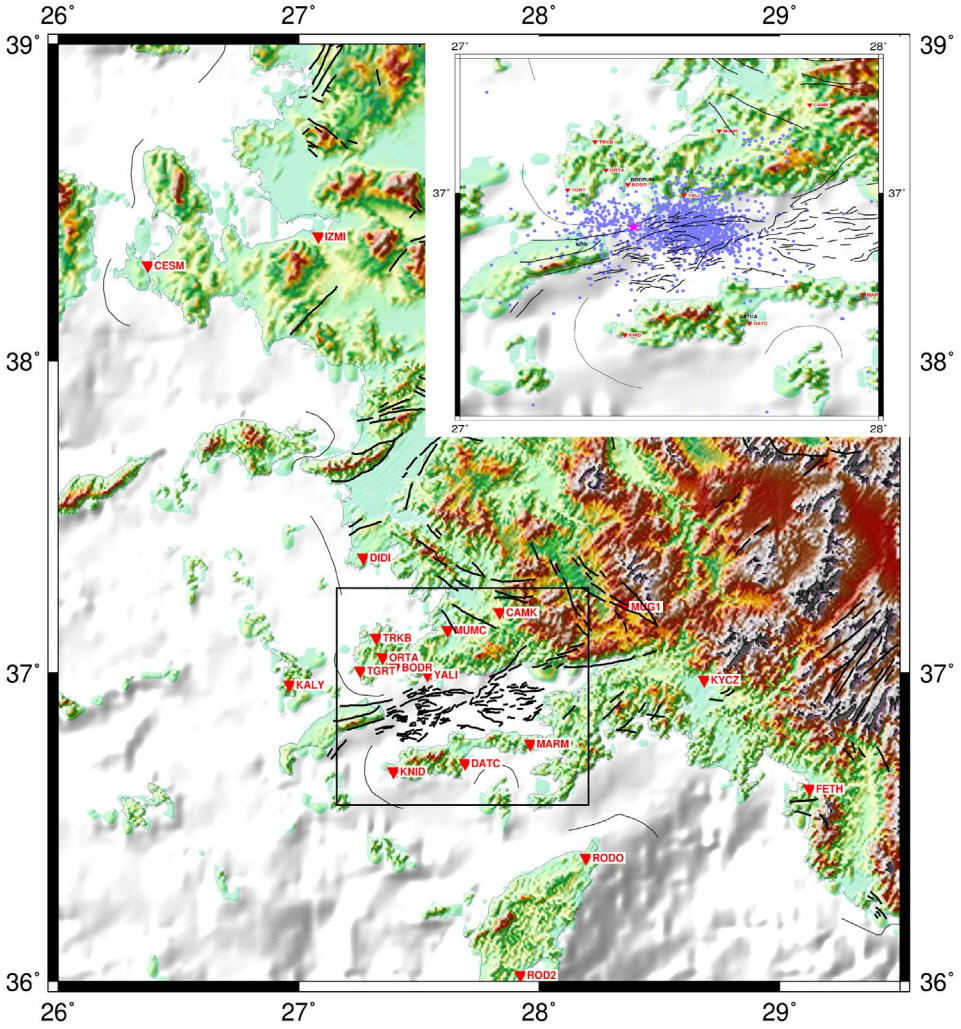


Figure 3. GPS network and aftershocks between Mw 2.0 and 5.0.

FES2004 Ocean Tide Loading (OTL) grid was used (Gulal, Erdogan, & Tiryakioglu, 2013; Herring, King, Floyd, & McClusky, 2015; Tiryakioglu et al., 2013). In this process, the daily coordinates were estimated from 15 IGS stations (TEHN, BAKU, KUWT, TELA, RAMO, CRAO, NICO, ANKR, GLSV, TUBI, ISTA, BUCU, SOFI, MATE, and GRAZ) with a stable time series (McClusky et al., 2000; Reilinger et al., 2006).

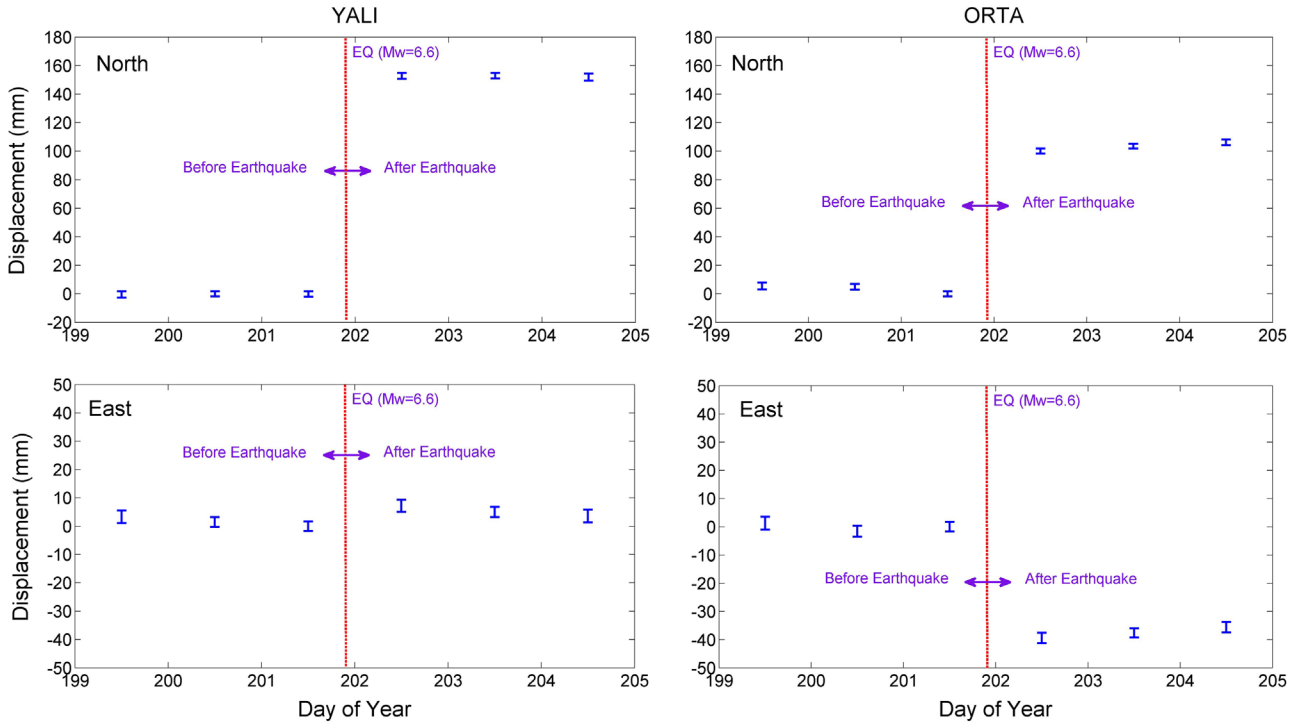


Figure 4. Observed coseismic displacements at YALI and ORTA sites.

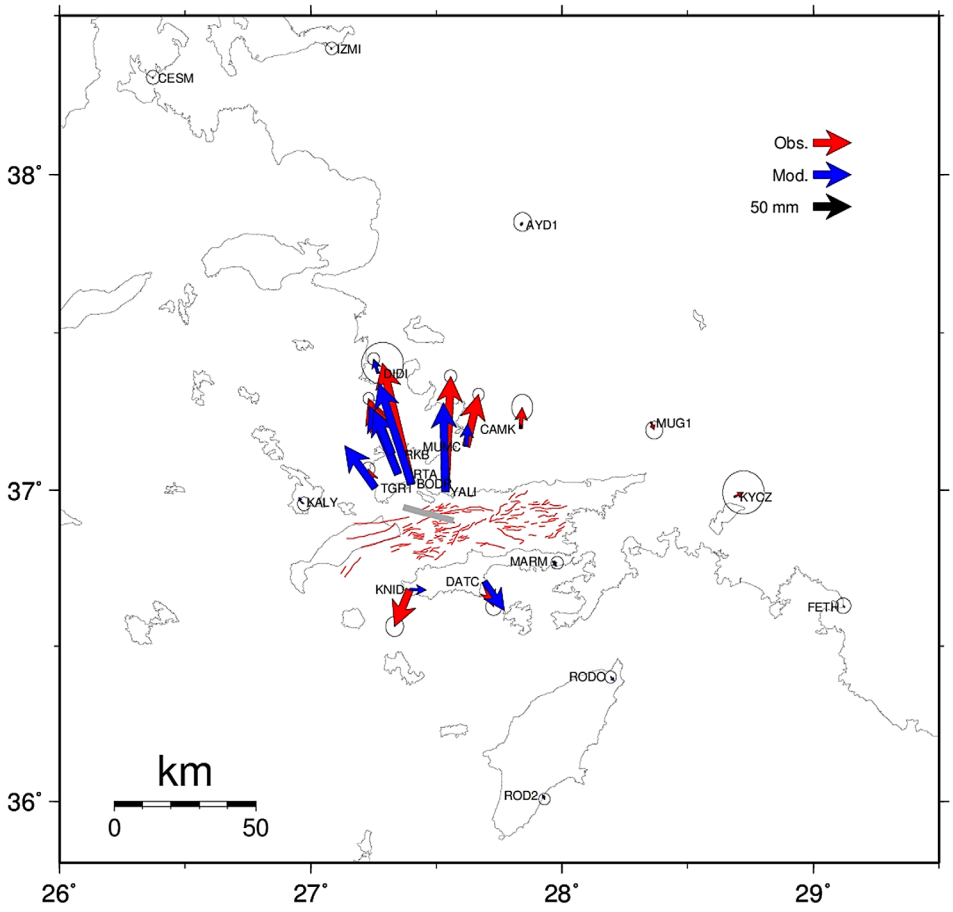


Figure 5. Observed and modeled coseismic displacements are shown in red and blue, respectively. Error ellipses are at %95 confidence level.

3.1.1. Coseismic displacements

Coseismic displacements are tightly correlated with the time series models. Short-term and long-term solution for the displacement are clearly exposed using continuous GPS data (Aktug et al., 2010; Tiryakioglu et al., 2017). The long-term evaluation is able to inform about the station movements which can be linear, periodic, irregular or episodic. On the contrary, short-term analysis is very conservative and stinted but it has more valuable information.

In this study, we analyzed the short-term daily solutions of continuous GPS in terms of the static coseismic displacements based on a scale in the Bodrum-Kos earthquake.

Because the earthquake occurred at 2017-07-20 01:31:12 (UTC), the estimation of the daily solution of the GPS sites on that day (DoY 201) did not include the data after the time of the earthquake. GPS data of MUMC station, one day before and after the earthquake, was not available. The MUMC station had a linear trend before the earthquake, which continued for approximately 1.5 years. The missing coordinates of MUMC station were estimated using the linear functions.

By comparing to the station position of the GPS sites from daily solutions before and after the Bodrum-Kos earthquake (DoY 201 and DoY 202), we obtained the coseismic displacement (Table 4).

The coseismic displacements from the short-term results were determined according to Equation (1).

$$\begin{aligned} \Delta e_{cos} &= e_{post}^{22\ hours} - e_{pre}^{24\ hours} \\ \Delta n_{cos} &= n_{post}^{22\ hours} - n_{pre}^{24\ hours} \\ \Delta h_{cos} &= h_{post}^{22\ hours} - h_{pre}^{24\ hours} \end{aligned} \tag{1}$$

where, Δe_{cos}, Δn_{cos}, Δh_{cos} is the permanent coseismic displacement, $e_{post}^{22\ hours}$, $n_{post}^{22\ hours}$, $h_{post}^{22hours}$ and $e_{pre}^{24\ hours}$, $n_{pre}^{24\ hours}$, $h_{pre}^{24\ hours}$ denote the positions estimated from GPS solutions based on 22 h (DoY 201) before and 24 h (DoY 202) after the earthquake, respectively.

Significant displacements have been observed, in particular for the stations near the epicenters (e.g. stations YALI, ORTA, TRKB, TGRT, DATC, BODR and DIDI). Uncertainties in coordinate differences were determined using standard error propagation. The observed horizontal and vertical displacements and uncertainties are illustrated in Figure 5 and Table 3.

As can be seen from the detected coseismic displacement in Table 3, the North components of these stations had more coseismic displacement than the East component. The coseismic displacements in the North component lie in the range of 19–160.2 mm, with uncertainties of 2.7–3.8 mm. Significant displacements in the East component lie in the range from 9.2 to 39.4 mm, with uncertainties 2.4–3.5 mm. There was no significant

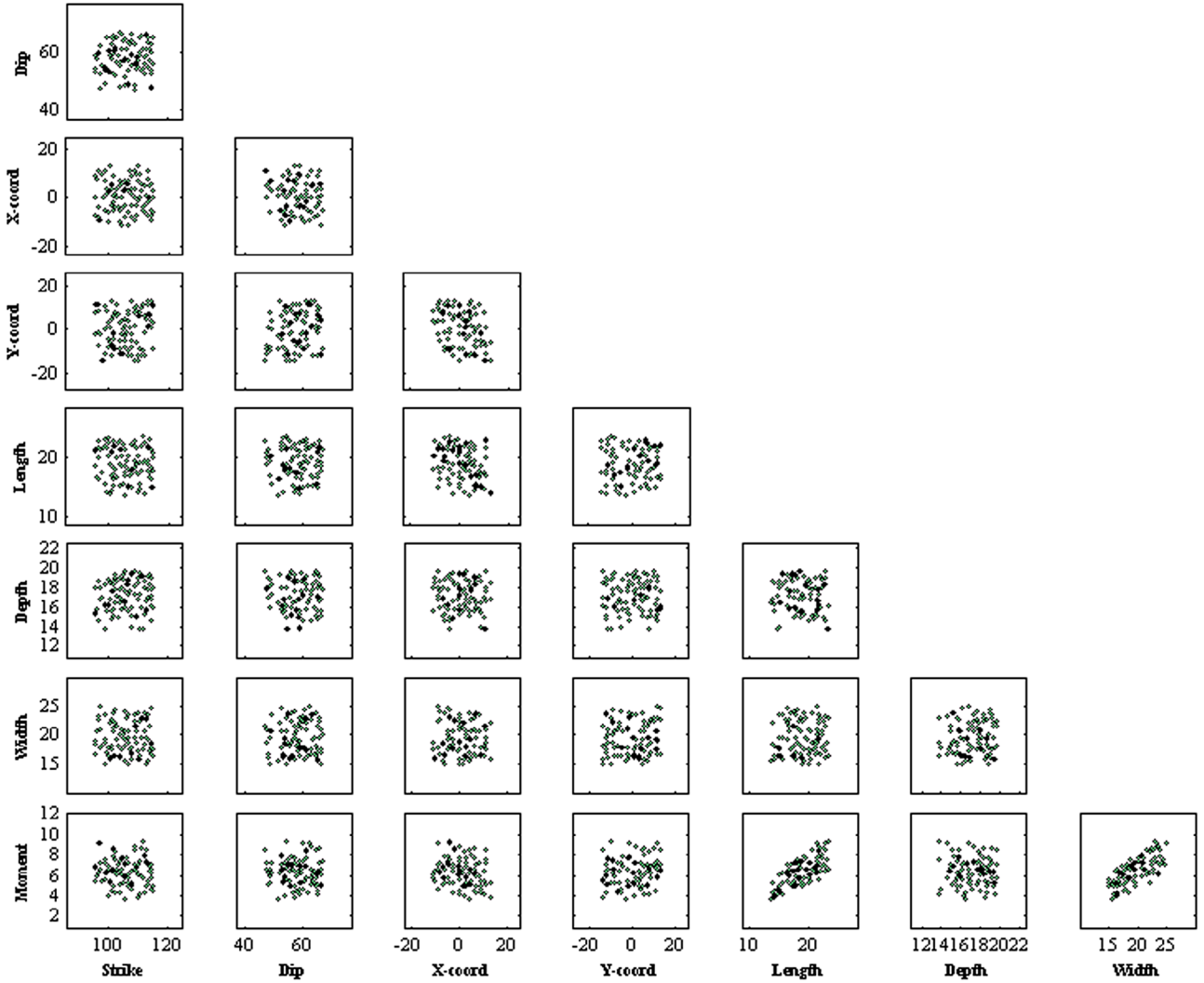


Figure 6. Model parameter trade-offs for the uniform-slip model. Each of the 100 dot in each of the plots is the best-fit solution to a different initial set of parameters. In these inversions, the fault slip is held fixed at 1 m. The values of the strike, dip are in degrees, moments are in 10^{25} dyne-cm, and all other parameters are in kilometers. The *X*-coordinate and *Y*-coordinate are along the east and the north direction, respectively and with respect to the reference point at 36.956N 28.370E. The depth is given from the surface. The moment is included as an auxiliary parameter since as the slip is fixed, the moment is not an independent parameter but instead a function of length and width.

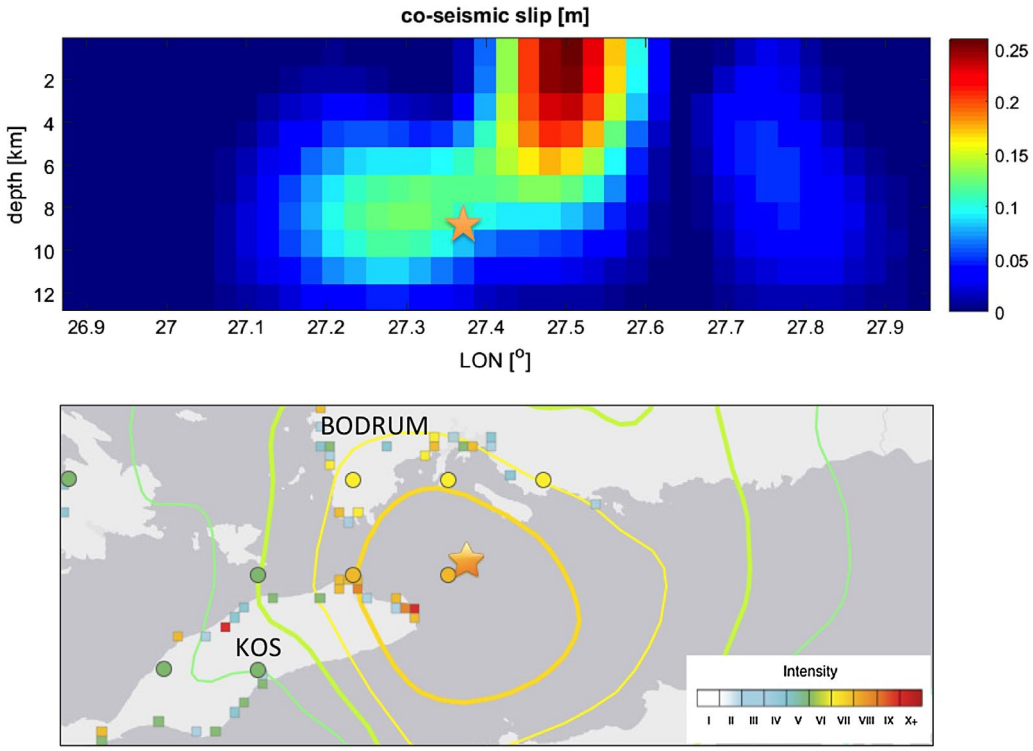


Figure 7. (Top) Along-fault distribution of co-seismic slip obtained from GPS-derived displacements. Mainshock hypocenter is shown by a yellow star. (Bottom) Intensity map of the 2017 Bodrum-Kos earthquake. Both graphs have the same longitudes.

coseismic displacement in the Up components of each station. From the results, we found that the maximum coseismic displacement of 160.2 mm in the North components occurred at station BODR. The estimated displacement in the East components of station BODR coseismic displacement of –38.3 mm. Station YALI had a coseismic displacement of 153.0 mm in the North components and in the East components of station YALI lie within its uncertainty.

Station ORTA had the coseismic displacement of 100.3, –39.4 mm at the North and East components, respectively. Stations MUMC and TRKB had the coseismic displacement of 69.1 mm, 23.3 mm and 64.9 mm, –24.9 mm at the North and East components, respectively. Stations TGRT and DATC had the coseismic displacement of 24.8 mm, –9.2 mm and –33.7 mm, 12.2 mm at the North and East components, respectively. Station DIDI had the least coseismic displacement of 18.9 mm at the North component. Furthermore, no significant coseismic displacement was observed in the remaining stations (MUG1, FETH, AYD1, CESM, IZMI, RODO, ROD2, KALY, CAMK, MARM, KYCZ and KNID).

3.2. Inversion modeling for the fault parameters

The GPS derived coseismic displacements were modeled as the surface displacements of a finite dislocation in an elastic half-space following Okada (1985). The relation between the surface displacements and the fault geometry parameters is nonlinear and involves many local minima. To invert the displacements for the fault geometry and slip rates, we adopted a hybrid optimization scheme which involves both global and local optimization. The details of the optimization strategy can be found in (Aktug et al., 2010). The objective function for the optimization was defined as the weighted residual sum of squares between the observed and the modeled displacements. While the relation between the surface displacements and the fault geometry is nonlinear, the slips on the dislocation are linearly related to the surface displacements. Therefore, we followed a two-step approach in the inversion. First, we inverted the coseismic displacements for the fault geometry assuming a uniform slip over the initial fault geometry. In the second step, we estimated the slip components fixing the fault geometry found in the first step.

The inversion method should be able to escape from the local minima and should be efficient. Our hybrid approach employs a global optimization scheme which employs simulated annealing to avoid local minima (Kirkpatrick, Gelatt, & Vecchi, 1983). However, as with all global optimization methods, the simulated annealing is not as efficient as quasi-Newton methods near global minimum. Therefore, the results were refined using a BFGS (Broyden–Fletcher–Goldfarb–Shanno) algorithm (Fletcher, 1987). The observed and modeled displacements are shown in Figure 5.

As opposed to the focal mechanisms obtained through seismometers, GPS derived fault mechanisms are unambiguous. Furthermore, the length and the width of the ruptured fault can be determined directly along with the slip components on the fault surface.

The obtained fault geometry and slip mechanism are given in Table 1. In general, the vertical offsets obtained from GPS measurements are noisier than horizontal components. There are various reasons for this including the constellation of GPS orbits and the seasonal effects which are the largest in the vertical component. Therefore, the vertical offsets are often well defined and their uncertainties are optimistic. To account for the possible contamination of the vertical component, we made the separate inversions, one with 2D displacements and one with 3D displacements.

Depending on the benchmark geometry, the slips are mostly correlated with the length and width of the fault. In this respect, in poor coverages with few sites, narrower and shorter faults with larger slips could give very similar results with those of wider and longer faults with smaller slips in the inversion (Aktug et al., 2010). The slip parameters are linearly related to the surface displacements as opposed to the geometry parameters displacements. In this respect, they can be estimated separately in a second step after all geometry parameters are resolved. The trade-offs between the geometry parameters are given in Figure 6.

3.3. Inversion for coseismic slip

'Steepest Decent/Gradient' inversion method is used to investigate co-seismic slip distribution along the rupture plane (Wang et al., 2009). The method employs Okada's semi-infinite space model to simulate elastic Green's functions in order to converge to the observed co-seismic displacements. We defined a grid space of 80 × 25 km along the rupture plane framing presumable high-slip patches. For the final results, data-model correlation is above %85. The inversion results are summarized in Figure 7 (top).

Co-seismic slip occurs on roughly a 65 km long and 25 km wide fault area. Maximum depth remains at 13 km in depth-sectional projection due to the inclined character of the normal fault. There are three high slip patches along the fault plane, where the co-seismic slips ranging between 0 and 26 cm. The western patch has a length of 25 km hosting co-seismic slips reaching up to 13 cm. Its center is well defined by the slip pattern at 8 km depth. It ruptures the depth range of 4–12 km. There is a smooth transition to the neighboring central patch, which has a length of 16 km. The central patch hosts the highest co-seismic slips reaching up to 26 cm. Its center is located much shallower at 3 km depth. It ruptures the depth range of 0–10 km. The eastern patch has a length of 18 km. It is clearly separated from the central patch. It hosts the lowest co-seismic slips remaining at 5 cm. Its center is located much at 6 km depth and it ruptures almost the entire depth range, from the surface to the basement of the seismogenic zone. Overall pattern indicates that the pre-earthquake coupling, which is storing the slip deficit, occurred on three patches.

The mainshock hypocenter is located at the transition between the western and the central high-slip patches. Referring to the hypocenter, which represents the nucleation point of the rupture, the activated fault hosts an asymmetrical coseismic slip distribution as it terminated at ~20 km to the west while it extended ~45 km to the east. Its highest slip patches are concentrated in the center as well as in the western section of the rupture, which is located between the longitudes 27.2°E and 27.6°E. This verifies the shake maps, where the highest ground shake is observed in the east of Kos and the south of Bodrum (Figure 7 bottom, source: https://earthquake.usgs.gov).

4. Conclusion

Combined GPS network consisting of GPS stations is used to capture coseismic displacements associated with the Bodrum-Kos earthquake (Mw6.6). Since the earthquake occurred offshore, the determination of source parameters using geodetic data is indispensable. Significant displacements have been observed, in particular, for the stations near the epicenter. The stations at a distance range of 13.5–50 km to the mainshock epicenter recorded coseismic displacements at ranges of 19–153 mm and 9.2–39.4 mm for the North and East components, respectively. Results showed that the mainshock generated more in N-S directed movement compared to the E-W direction. This is well correlated with a N-S extending and EW striking normal-type focal mechanism . We have not observed a significant coseismic displacement in the Up components. Furthermore, no significant coseismic displacement have been observed in the stations that are more than 50 km away from the epicenter.

The mainshock activated a ~65 km long and 25 km wide inclined fault area which dips down to 13 km depth. The rupture has three high-slip patches, namely western, central and eastern patches, where the co-seismic slips reach up to 13, 26 and 5 cm, respectively. This slip pattern indicates that the pre-earthquake coupling, which is storing the slip deficit, occurred on these three patches. The highest pre-earthquake coupling has probably occured in central patch. Mainshock nucleation point remains between the western and central patches. The ruptured has an asymmetrical distribution of coseismic slips referring to the hypocenter as it terminated at ~20 km in the west while it extended for ~45 km to the east.

As opposed to the large on-land earthquakes, where surface observations are also available, earthquakes of moderate size are, in particular offshore requires a good observation coverage. KOERI and AFAD, which operates national seismic networks in Turkey, revised their magnitudes up to 0.5, which presents a large uncertainty for source parameters of such a large size earthquake. Accordingly, coseismic geodetic displacements are relatively small to be determined in survey-type measurements and a continuous monitoring is needed. In this

study, one of the earliest examples of contributions of the new CORS-TR to the earthquake geodesy in Turkey is presented, in particular at a large size earthquake.

Combining GPS observations with surface geological data, we conclude the fault geometry from the surface to depths of about 17 km has listric characters. The main shock and aftershocks of the 2017 Bodrum-Kos earthquake suggest that the fault mechanism can be classified into two groups based on focal mechanism solutions. (1) NE-trending oblique- to strike-slip faults with moderate-depth hypocenters (up to 14 km) at the western end of the GFZ, (2) approximately E-W trending normal faults with shallow earthquakes (up to 17 km) at the middle and western section of GFZ.

The instrumental period earthquakes suggest a westward propagation along the GFZ. Source mechanism solutions for most of these earthquakes indicate that normal fault mechanisms with a small strike-slip component have been observed on the E–W-oriented normal fault systems in the Gulf of Gökova, which confirms that the extension is in a north-south direction.

Acknowledgements

GPS data used in this study are integrated from CORS-TR (TUSAGA-Aktif), NOANET Greece, Tree Company Co., and Independent Geomatic Engineers Office-Bodrum. Authors thank George Polykretis for providing data from Tree Company CO. GPS network. Authors thank Editor Erdin Bozkurt and anonymous referee for constructive review process.

Disclosure statement

No potential conflict of interest was reported by the authors.

Funding

This work was supportted by Research Foundation of Afyon Kocatepe University [project number 17.FEN.BIL.35].

ORCID

B. Aktuğ http://orcid.org/0000-0002-7995-4477
C. Ö. Yiğit http://orcid.org/0000-0002-1942-7667
Ç Özkaymak http://orcid.org/0000-0002-0377-1324
E. Taneli http://orcid.org/0000-0002-1252-8908
F. Bulut http://orcid.org/0000-0001-8108-8881
A. Doğru http://orcid.org/0000-0002-1930-6443
H. Özener http://orcid.org/0000-0003-2531-3030

References

Aktug, B., Kaypak, B., & Çelik, R. N. (2010). Source parameters of 03 February 2002 Çay Earthquake, Mw6.6 and aftershocks from GPS Data, Southwestern Turkey. *Journal of Seismology, 14*, 445–456.

Aktug, B., Nocquet, J. M., Cingoz, A., Parsons, B., Erkan, Y., England, P. C., … Tekgul, A. (2009). Deformation of western Turkey from a combination of permanent and campaign GPS data: Limits to block-like behavior. *Journal of Geophysical Research, 114*, B10404.

Altinok, Y., & Ersoy, S. (2000). Tsunamis observed on and near the Turkish coast. *Natural Hazards, 21*, 185–205.

Ambraseys, N. N., & White, D. (1997). The seismicity of the eastern Mediterranean region 550-1 BC: a re-appraisal. *Journal of Earthquake Engineering, 1*, 603–632.

Bozkurt, E. (2001). Neotectonics of Turkey: A synthesis. *Geodinamica Acta, 14*, 3–30.

Brun, J. P., Faccenna, C., Gueydan, F., Sokoutis, D., Philippon, M., Kydonakis, K., & Gorini, C. (2016). The two-stage Aegean extension, from localized to distributed, a result of slab rollback acceleration. *Canadian journal of earth sciences, National Research Council Canada, 53*(11), 1142–1157.

Ciftci, N. B., & Bozkurt, E. (2010). Structural evolution of the Gediz Graben, SW Turkey: Temporal and spatial variation of the Graben basin. *Basin Research, 22*, 846–873.

DDA. (2017). *Disaster and Emergency Management Presidency, Earthquake Department – Ankara, Turkey*. Retrieved from http://www.deprem.gov.tr/

Dewey, J. F., & Şengor, A. M. C. (1979). Aegean and surrounding regions: Complex multiplate and continuum tectonics in a convergent zone. *Geological Society of America Bulletin, 90*, 89–92.

Dogru, A., Gorgun, E., Ozener, H., & Aktug, B. (2014). Geodetic and seismological investigation of crustal deformation near Izmir (Western Anatolia). *Journal of Asian Earth Sciences, 82*, 21–31.

Duman, T. Y., Emre, O., Ozalp, S., & Elmacı, H. (2011). *1:250.000 scale Active Fault Map Series of Turkey, Aydın (NJ35-11) Quadrangle* (Serial Number:7). Ankara: General Directorate of Mineral Research and Exploration.

Emre, O., Duman, T. Y., & Ozalp, S. (2011). *1:250.000 scale Active Fault Map Series of Turkey, Marmaris (NJ35-15) Quadrangle* (Serial Number:78). Ankara: General Directorate of Mineral Research and Exploration.

EMSC. (2017). *European-Mediterranean Seismological Centre*. Retrieved from http://www.emsc-csem.org

Eyidogan, H., Akinci, A., Gündogdu, O., Polat, O., & Kaypak, B. (1996, February 8–9). Investigation of the recent seismic activity of Gökova Basin. In *Proceedings of National Marine Geology and Geophysical Programme Workshop I* (pp. 68–71). Izmir.

Fletcher, R. (1987). *Practical methods of optimization* (2nd ed.). New York: Wiley. ISBN 978-0-471-91547-8.

GFZ. (2017). *GeoForschungsZentrum (GFZ-Potsdam) – Potsdam, Germany*. Retrieved from http://www.gfz-potsdam.de/geofon

Gorur, N., Sengor, A. M. C., Sakinc, M., Tuysuz, O., Akkok, R., Yigitbas, E., & Aykol, A. (1995). Rift formation in the Gokova region, southwest Anatolia: implications for the opening of the Aegean Sea. *Geological Magazine, 132*, 637–650.

Guidoboni, E., Comastri, A., & Triana, G. (1994). *Catalogue of Ancient Earthquakes in the Mediterranean Area up to the 10th century*. Rome: Instituto Nazionale di Geofisica.

Gulal, E., Erdogan, H., & Tiryakioglu, I. (2013). Research on the stability analysis of GPS reference stations network by time series analysis. *Digital Signal Processing, 23*, 1945–1957. doi:10.1016/j.dsp.2013.06.014

Gurer, O. F., Sangu, E., Ozburan, M., Gurbuz, A., & Sarica-Filoreau, N. (2013). Complex basin evolution in the Gökova Gulf region: implications on the Late Cenozoic tectonics of southwest Turkey. *International Journal of Earth Sciences, 102*, 2199–2221.

Herring, T. A., King, R. W., Floyd, M. A., & McClusky, S. C. (2015). GAMIT/GLOBK reference manual. *Release 10.6* Cambridge, MA.

HRV. (2017). *The Harvard Centroid Moment Tensor Catalog*. Retrieved from http://www.globalcmt.org/

Iscan, Y., Tur, H., & Gokasan, E. (2013). Morphologic and seismic features of the Gulf of Gökova, sw anatolia: Evidence of strike-slip faulting with compression in the Aegean Extensional Regime. *Geo-Marine Letters, 33*, 31–48.

Jackson, J., & McKenzie, D. (1984). Active tectonics of the Alpine-Himalayan belt between Western Turkey and Pakistan. *Geophysıcs Journal of Royal Astronomy Society, 77*, 185–264.

Jolivet, L., & Brun, J. P. (2010). Cenozoic geodynamic evolution of the Aegean. *International Journal of Earth Sciences, 99*, 109–138.

Kalafat, D., & Horasan, G. (2012). A seismological view to Gökova region at southwestern Turkey. *International Journal of Physics Science, 7*(30), 5143–5153.

Kaymakci, N. (2006). Kinematic development and paleostress analysis of the Denizli Basin (Western Turkey): Implications of spatial variation of relative paleostress magnitudes and orientations. *Journal of Asian Earth Sciences, 27*, 207–222.

Kirkpatrick, S., Gelatt, C. D., Jr., & Vecchi, M. P. (1983). Optimization by simulated annealing. *Science, 220*(4598), 671–680.

Kocyigit, A., & Deveci, S. (2007). A N-S-trending avtive extensional structure, the Suhut (Afyon) graben: Commencement age of the extensional neotectonic period in the Isparta Angle, SW Turkey. *Turkish Journal of Earth Sciences, 16*, 391–416.

KOERI. (2017). *Kandilli Observatory and Earthquake Research Institute – Istanbul, Turkey*. Retrieved from http://www.koeri.boun.edu.tr/

Konak, N., & Senel, M. (2002). *Geological map of Turkey in 1/500.000 scale, Denizli sheet*. Ankara: Publication of Mineral Research and Exploration Directorate.

Kurt, H., Demirbag, E., & Kuscu, I. (1999). Investigation of submarine active tectonism in the Gulf of Gökova, southwest Anatolia – SE Aegean Sea, by multi-channel seismic reflection data. *Tectonophysics, 305*, 477–496.

Le Pichon, X., Chamot-Rooke, N., Lallemant, S., Noomen, R., & Veis, G. (1995). Geodetic determination of the kinematics of central Greece with respect to Europe: impli-cations for eastern Mediterranean tectonics. *Journal of Geophysical Research, 100*, 12675–12690.

Lisowski, M. (1997). Postseismic strain following the 1989 Loma Prieta earthquake from GPS and leveling measurements. *Journal of Geophysical Research, 102*, 4933–4955.

Luttrell, A. (1999). Earthquakes in the Dodecanese: 1303–1512. In E. Zachariadon (Ed.), Natural Disasters in the Ottoman Empire (Rethymnon, 1999), repr. İn Luttrell, Studies, no. X, pp 145-51

McClusky, S., Balassanian, S., Barka, A., Demir, C., Ergintav, S., Georgiev, I., Gurkan, O., … Veis, G. (2000). Global Positioning System constraints on plate kinematics and dynamics in the eastern Mediterranean and Caucasus. *Journal of Geophysical Research-Solid Earth, 105*, 5695–5719. doi:10.1029/1999jb900351.

McKenzie, D. P. (1972). Active tectonics of the Mediterranean region. *Geophysical Journal of the Royal Astronomical Society, 30*, 109–185.

NOA. (2017). *National Observatory of Athens, Geodynamic Institute – Athens, Greece*. Retrieved from http://bbnet.gein.noa.gr/

Okada, Y. (1985). Surface deformation due to shear and tensile faults in a half-space. *Bulletin of the Seismological Society of America, 75*, 1135–1154.

Ozener, H., Dogru, A., & Acar, M. (2013). Determination of the displacements along the Tuzla fault (Aegean region-Turkey): Preliminary results from GPS and precise leveling techniques. *Journal of Geodynamics, 67*, 13–20.

Ozkaymak, C. (2015). Tectonic analysis of the Honaz Fault (western Anatolia) using geomorphic indices and the regional implications. *Geodinamica Acta, 27*, 110–129. doi :10.1080/09853111.2014.957504

Ozkaymak, C., Sozbilir, H., & Uzel, B. (2013). Neogene-Quaternary evolution of the Manisa Basin: Evidence for variation in the stress pattern of the İzmir-Balıkesir Transfer Zone, western Anatolia. *Journal of Geodynamics, 65*, 117–135.

Reddy, C. D., & Sunil, P. S. (2008). Post-seismic crustal deformation and strain rate in Bhuj region, western India, after the 2001 January 26 earthquake. *Geophysical Journal International, 172*(2), 593–606.

Reilinger, R., McClusky, S., Paradissis, D., Ergintav, S., & Vernant, P. (2010). Geodetic constraints on the tectonic evolution of the Aegean region and strain accumulation along the Hellenic subduction zone. *Tectonophysics, 488*(1–4), 22–30. doi:10.1016/j.tecto.2009.05.027

Reilinger, R., McClusky, S., Vernant, P., Lawrence, S., Ergintav, S., Cakmak, R., … Karam, G. (2006). GPS constraints on continental deformation in the Africa-Arabia-Eurasia continental collision zone and implications for the dynamics of plate interactions. *Journal of Geophysical Research, 111*, B05411.

Saroglu, F., Emre, O., & Kuşçu, İ. (1992). *Active fault map of Turkey (in Turkish). Scale 1:2.000.000*. Ankara: Mineral Research Exploration of Turkey Press.

Sengor, A. M. C. (1987). Cross-faults and differential stetching of hanging walls in regions of low-angle normal faulting: Examples from western Turkey. In: M. P. Coward, J. F. Dewey, & P. Hancock (Eds.), *Continental extensional tectonics* (pp. 575–589). London: Geological Society'de. Special Publication, 28.

Sozbilir, H., Sari, B., Uzel, B., Sumer, O., & Akkiraz, S. (2011). Tectonic implications of transtensional supradetachment basin development in an extension-parallel transfer zone: the Kocaçay Basin, western Anatolia, Turkey. *Basin Research, 23*, 423–448.

Stiros, S. C. (2000). Fault pattern of Nisyros Island volcano (Aegean Sea, Greece): Structural, coastal and archaeological evidence. In: W. J. McGuire, D. R. Griffiths, P. L. Hancock, & I. S. Stewart (Eds.), *The archaeology of geological catastrophes* (pp. 385–399). London: Geological Society. Special Publications 171.

Tiryakioglu, I. (2015). Geodetic aspects of the 19 May 2011 Simav earthquake in Turkey. *Geomatics, Natural Hazards and Risk, 6*(1), 76–89.

Tiryakioglu, I., Floyd, M., Erdogan, S., Gulal, E., Ergintav, S., McClusky, S., & Reilinger, R. (2013). GPS constraints on active deformation in the Isparta Angle region of SW Turkey. *Geophysical Journal International, 195*, 1455–1463.

Tiryakioglu, I., Yigit, C. O., Yavaşoglu, H., Saka, M. H., & Alkan, R. M. (2017). The determination of interseismic, coseismic and postseismic deformations caused by the Gökçeada-Samothraki earthquake (2014, Mw: 6.9) based on GPS data. *Journal of African Earth Sciences, 133*(2017), 86–94.

Tur, H., Yaltirak, C., Elitez, İ., & Sarikavak, K. (2015). Pliocene-Quaternary tectonic evolution of the Gulf of Gökova, southwest Turkey. *Tectonophysics, 638*, 158–176.

Ulug, A., Duman, M., Ersoy, S., Ozel, E., & Avci, M. (2005). Late Quaternary sea-level change, sedimentation and neotectonics of the Gulf of Gökova: Southeastern Aegean Sea. *Marine Geology, 221*, 381–395.

Wang, L., Wang, R., Roth, F., Enescu, B., Hainzl, S., & Ergintav, S. (2009). Afterslip and viscoelastic relaxation following the 1999 M 7.4 Izmit earthquake from GPS measurements. *Geophysical Journal International, 178*(3), 1220–1237.

Yilmaz, Y., Genc, S. C., Gurer, O. F., Bozcu, M., Yilmaz, K., Karacik, Z., … Elmas, A. (2000). When did the western Anatolian grabens begin to develop? In E. Bozkurt, J. A. Winchester, & J. D. A. Piper (Eds.), *Tectonics and magmatism in Turkey and the surrounding area* (pp. 353–384). London: Geological Society of London, Special Publication 173.

Yolsal, S., & Taymaz, T. (2010). Source mechanism parameters of Gulf of Gökova earthquakes and tsunami risk in the Rodos-Dalaman region. *ITU Dergisi/d* (Vol. 9(3), pp. 53–65). Istanbul: Istanbul Technical University.

Yolsal, S., & Taymaz, T. (2012). Earthquake source parameters along the Hellenic subduction zone and numerical simulations of historical tsunamis in the Eastern Mediterranean. *Tectonophysics, 536–537*, 61–100.

Yolsal, S., Taymaz, T., & Helvaci, C. (2014). Earthquake mechanisms in the Gulfs of Gökova, Sığacık, Kuşadası, and the Simav Region (western Turkey): Neotectonics, seismotectonics and geodynamic implications. *Tectonophysics, 635*, 100–124.

Yolsal, S., Taymaz, T., & Yalciner, A. C. (2007). Understanding tsunamis, potential source regions and tsunami prone mechanisms in the Eastern Mediterranean. In: T. Taymaz, Y. Yilmaz, & Y. Dilek (Eds.), *The geodynamics of the Aegean and Anatolia* (pp. 201–230). London: Geological Society. Special Publications, 291.